Research Article | Vol. 11, No. 5 / 1 May 2020 / Biomedical Optics Express 2578
Biomedical Optics EXPRESS

Remote scanning for ultra-large field of view in wide-field microscopy and full-field OCT

GAËLLE RECHER,[1,2] PIERRE NASSOY,[1,2] AND AMAURY BADON[1,2,*]

[1] LP2N, Laboratoire Photonique Numérique et Nanosciences, Univ. Bordeaux, F-33400 Talence, France
[2] Institut d'Optique Graduate School & CNRS UMR 5298, F-33400 Talence, France
[*] amaury.badon@institutoptique.fr

Abstract: Imaging specimens over large scales and with a sub-micron resolution is instrumental to biomedical research. Yet, the number of pixels to form such an image usually exceeds the number of pixels provided by conventional cameras. Although most microscopes are equipped with a motorized stage to displace the specimen and acquire the image tile-by-tile, we propose an alternative strategy that does not require to move any part in the sample plane. We propose to add a scanning mechanism in the detection unit of the microscope to collect sequentially different sub-areas of the field of view. Our approach, called remote scanning, is compatible with all camera-based microscopes. We evaluate the performances in both wide-field microscopy and full-field optical coherence tomography and we show that a field of view of 2.2×2.2 mm^2 with a 1.1 μm resolution can be acquired. We finally demonstrate that the method is especially suited to image motion-sensitive samples and large biological samples such as millimetric engineered tissues.

1. Introduction

Deciphering biological processes often relies on the dual ability to perform *in toto* three-dimensional imaging of the sample, which can be of macroscopic size, and to reach a sub-cellular (i.e. $\sim \mu$m) resolution. Amongst all available biomedical imaging techniques, optical microscopy, which is characterized by a high spatial resolution and a moderate invasiveness, is undoubtedly a good candidate. In the recent years, most efforts have focused on developing strategies to image living samples in depth. However, imaging large volumes with sub-micron resolution also raises an issue that has been often overlooked, namely the limited amount of information that can be captured by a microscope.

It is common to consider that the microscope objective (MO) is the primary limiting factor of a microscope throughput. Indeed, we all experienced that a high magnification MO provides a small field of view (FOV) at high lateral resolution, while a low magnification MO would expand the FOV but with a degraded resolution. Quantitatively, the spatial bandwidth product (SBP) characterizes the throughput of an objective. It is defined as the number of pixels necessary to capture the full FOV at Nyquist sampling [1–3]. As a reference point, a standard X10 with a 1.1 μm resolution and a theoretical 2.65×2.65 mm^2 FOV has an SBP of 21 megapixels. This number already exceeds the typical number of pixels on a camera, commonly between 1 and 4 megapixels, meaning that detectors are actually the limiting factor and that most of the information captured and transmitted by a MO is simply discarded.

As numerous biomedical applications require a large FOV, the SBP of a microscope is usually increased by mechanically scanning the sample laterally, acquiring images for various positions and finally stitching them. Yet, moving the specimen stage with accuracy is intrinsically a slow process that could furthermore be challenging in the case of bulky specimens or mounts. More importantly, this can induce problematic sample motion when the sample is positioned in an culture or immersion medium. For instance, spherical capsules containing cells are especially

#383329 https://doi.org/10.1364/BOE.383329
Journal © 2020 Received 25 Nov 2019; revised 4 Apr 2020; accepted 6 Apr 2020; published 16 Apr 2020

Biomedical Optics EXPRESS

sensitive to any displacement of the sample stage. These specimens can be obtained with a microfluidics technique called the cellular capsule technology (CCT) which produces at high rate 3D structures made of a suspension of cells inside a porous membrane [4]. Depending on the nature of the cells encapsulated, these specimens are valuable to recapitulate the 3D architecture and function of various living tissues [5] or to understand mechanotransduction mechanisms in tumor formation for instance [6].

In this article, we report on a simple method to significantly increase the FOV of a camera-based microscope without moving the sample in the focal plane of the MO. Our technique is inspired by the optical scanning microscope which proposed to enlarge the lateral FOV of a custom-built MO by using a scanning mirror in the Fourier plane [7,8]. Here, we propose a novel imaging method that combines the advantages of this previous approach with full-field optical coherence tomography (FF-OCT) [9,10] to perform volumetric imaging on the millimeter scale with a micrometer resolution and without moving the specimen in any dimension. Practically, a mirror on a motorized kinematic mount is added in the detection part of a FF-OCT apparatus. While FF-OCT provides axial scanning by simply moving the mirror in the reference arm, similarly to remote focusing [11], angular scanning in the detection part is translated by a lateral shift of the detected FOV. A series of different tilt angles allows the sequential acquisition of diffraction limited images corresponding to different areas of the microscope lateral FOV. By stitching them, we nearly cover the full microscope FOV resulting in a throughput of around 16 MPixels. We demonstrate the benefits of this technique to image capsules and large 3D biological samples.

2. Results

2.1. Imaging encapsulated cells with wide-field microscopy and FF-OCT

A label-free and tri-dimensional imaging method is necessary to both characterize the shape and the structure of the capsules and to monitor their growth over relatively long periods, typically several days. FF-OCT combines both of these requirements, low photodamage and optical sectioning, by using a low-coherence light source and an interferometric detection. These assets have already been used to observe non-invasively the development of retinal organoids [12].

Figure 1(a) shows a schematic of the initial experimental set-up which combines two modalities: wide-field microscopy and FF-OCT. A broadband and spatially incoherent light source centered at 660 nm (M660L4, Thorlabs) illuminates a Michelson interferometer in a Kohler configuration made of four lenses and two apertures. Light is separated by a beam splitter (CCM1-BS013, Thorlabs) and propagates through two identical MO (UMPLFLN 10X, Olympus) placed in the two arms. The specimen of interest is placed in the focal plane of one of the MO while a silicon mirror is positioned in the second arm. The latter is supported by a piezoelectric transducer (PZT) which modulates the optical path difference between the two interferometric arms. Light reflected in the two arms is then collected by the same MO, focused by a tube lens (AC508-400-A-ML, f=400 mm, Thorlabs) and imaged by a CMOS camera (MV1-D1024E-160-CL-12, PhotonFocus). Figure 1 displays typical images of a single capsule containing liver cells obtained with our setup. While the wide-field mode provides a contrasted image of the specimen, the lack of optical sectioning prevent to provide any volumetric information on the shape of the capsule or the structure of the cell aggregate. Alternatively, the structure of the capsule can be imaged at any depth with the FF-OCT mode. Both the encapsulated cells and the interfaces with the inside and outside of the capsule are visible. The en-face images obtained at various depths were obtained by just moving the mirror in the focal plane of the reference arm, similarly to remote focusing [11]. Yet, our approach is here constrained by the limited FOV due to the finite number of pixels of the camera. In our configuration, only a single capsule is imaged when Nyquist sampling is full-filled. Thus, imaging an ensemble of capsules or larger structures requires to increase this FOV.

Biomedical Optics EXPRESS

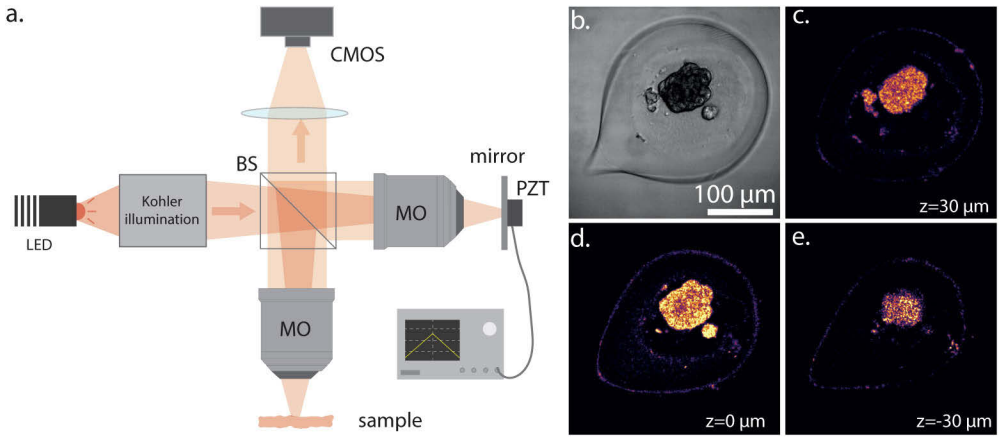

Fig. 1. Imaging capsules with wide-field microscopy and full-field optical coherence tomography. (a) Optical setup. MO, microscope objective; BS, beam splitter; M, mirror; PZT, piezoelectric transducer. (b) Wide-field image of a capsule containing liver cells. (c-e) FF-OCT images of the same capsule for depths equal to 30, 0 and -30 μm respectively. Scale bar, 100 μm

2.2. Motion artifact with mechanical scanning

Conventionally, increasing the FOV is done by mechanically scanning the sample with a motorized stage. While this technique has the advantage of potentially providing an infinite FOV, the translation of the sample can have detrimental effects. Here, our specimens of interest are made of cells encapsulated into a porous alginate shell. Due to their geometry and the need to keep them in both a culture medium and a stress-free environment (preventing us from embedding them in an additional hydrogel), these specimens are sensitive to motion. Figure 2 displays a typical example of what happens when the sample is scanned using a motorized stage (see also Visualization 1). After moving the sample 500 μm to the left and going back to its initial position, the capsule exhibits a slow rotation. This effect is an issue for several reasons. First, the drift of the sample is detrimental for long-term imaging and tracking, as its position evolves as a function of time. In addition, all the capsules are not affected in the same way by this drift as they differ in size, weight and orientation. On Fig. 2(a), only the capsule on top rotates while the capsule on the bottom of the image remains static. Hence, post-acquisition global compensation of the drift can not be performed. Secondly, the cellular inner core is fragile and any shear or unwanted stress may alter the behaviour of the fate of cells. Such a perturbative scanning makes the approach incompatible with long-term imaging. Finally, this drift due to the inertial accumulation of kinetic energy is particularly problematic for FF-OCT acquisition. Indeed, OCT images are obtained from a combination of intensity images while varying the reference mirror position. If the sample is moving during an acquisition, artifacts will appear and corrupt the results.

2.3. Principle of remote scanning

To perform volumetric imaging over a large lateral FOV and without moving the sample, we implement the remote scanning approach on a FF-OCT system. Here, we propose to take advantage of the mismatch between the FOV of the MO and the smaller area detected by the camera (see Fig. 3(a)). Figure 3(d) shows a schematic of the modified experimental set-up. Compared to the initial system, a two-axes motorized mirror mount (KS1-Z8, Thorlabs) is simply added in the Fourier space of the detection arm of the microscope. In practice, access to Fourier space in the detection is obtained by using an afocal system of magnification 1 (not shown in

Biomedical Optics EXPRESS

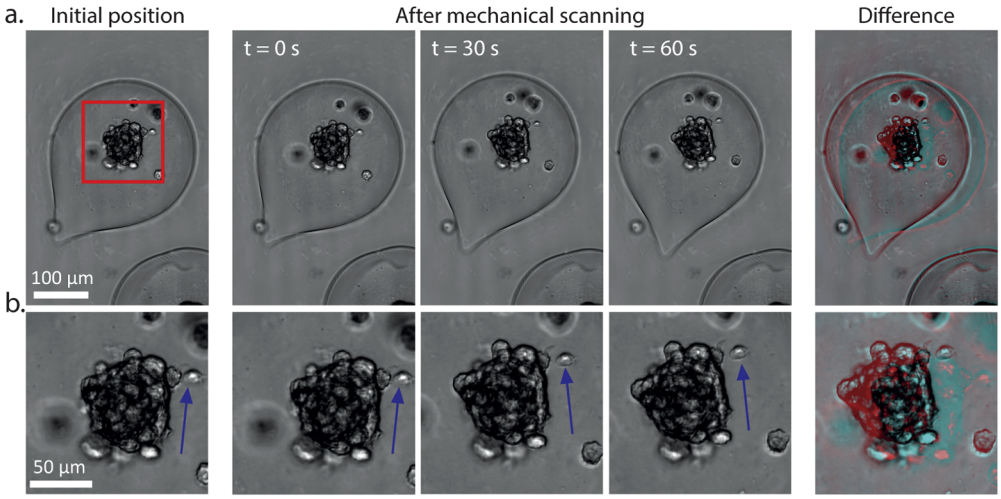

Fig. 2. Effect of mechanical scanning when imaging capsules with wide-field microscopy. (a) The sample is mechanically scanned to the left with a motorized stage. After going back to its initial position, the capsules slowly rotates in the immersion medium. (b) Zoom in of the area corresponding to the red square in (a). In addition of the global motion of the capsule, the inner supracellular structure is also affected. As indicated by the blue arrow, a cell splits off the central cell aggregate.

Fig. 3.d). Because the scanning system is in the Fourier space, a tilt of the mirror is solely translated into a shift of the image in the camera plane, without introducing any time-delay or image distortion. To cover the full FOV of the MO, a scan is performed by applying a series of two-dimensional tilts to the mirror (Fig. 3(d)).

2.4. Optical performances

To characterize our optical system in the wide-field microscopy mode, we first imaged a positive USAF 1951 resolution target. By tilting the mirror in the detection unit, 7×7 wide-field images corresponding to different areas of the sample are collected. After stitching these images into a mosaic, a FOV covering 2.2×2.2 mm^2 is obtained with a diffraction limited resolution, here 1.1 μm. On the edges of the FOV, we observe a slight loss of signal corresponding to the limits of the field of full light and only a moderate transverse resolution degradation (see Appendix D).

Secondly, we assessed the performances of the remote scanning applied to the FF-OCT system. By axially moving the mirror in the reference arm of the interferometer, a z-stack is acquired for each position of the scanning mirror. For each axial position, the electromagnetic field is computed from intensity measurements using a phase shifting interferometry technique (see Appendix A). While the transverse resolution is limited by the numerical aperture of the MO, similarly to the wide-field mode, the axial resolution is given by the coherence length of the light source. Indeed, interferences disappear if the optical path length between the two arms is larger than this physical value. The axial resolution is then estimated as the full width at half maximum (FWHM) of the interferometric signal amplitude (Fig. 4(b)). From the stacks acquired for the various angles of the scanning unit, the axial resolution is estimated for all the locations of the FOV. As seen in the resolution map shown in Fig. 4(d), our system presents an axial resolution of 5.6 μm on average. This value matches the coherence length of the LED used as a light source. Notably, no degradation of the axial resolution is observed on the edges of the FOV.

Finally, the position of the peak in the interferometric signal indicates the axial position of focus. As seen in Fig. 4(c), there is a shift of 6 μm from the left to the right of the image. We

Biomedical Optics EXPRESS

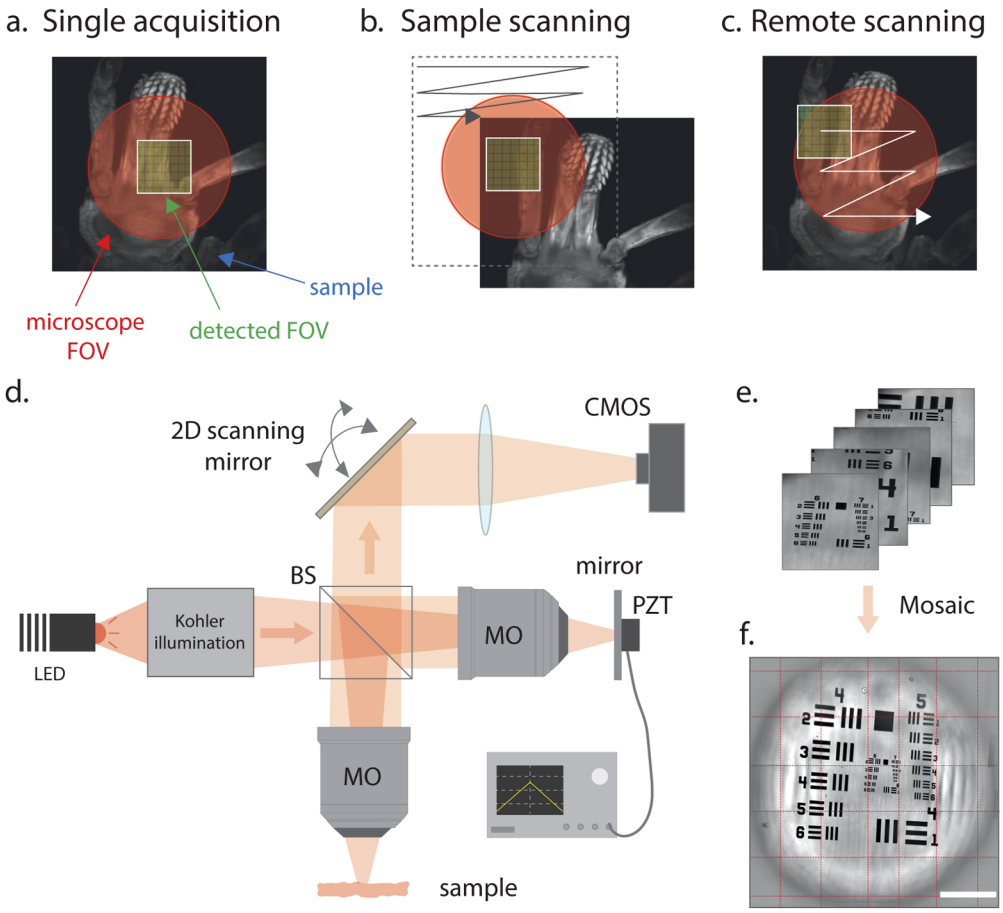

Fig. 3. Principle of the remote scanning approach. (a) With a conventional microscope, the recorded FOV is limited by the detected area which is usually much smaller than the accessible FOV of the MO. (b) The simplest solution to enlarge the FOV consists in moving the specimen and keeping the detection still. (c) Alternatively, access to a larger FOV can be obtained by scanning the detected area across the FOV accessible by the MO, the specimen remaining stationary. (d) Optical setup. A motorized mirror placed in the Fourier space in the detection unit allows to scan different regions in the accessible FOV. (e,f) A stack of images is rearranged as a mosaic to obtain a large FOV. Scale bar, 500 μm

Biomedical Optics EXPRESS

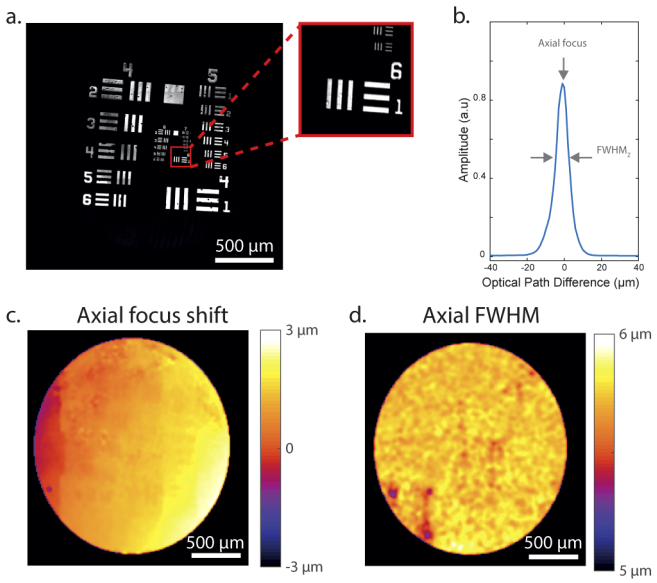

Fig. 4. Optical performances of the remote scanning unit applied on FF-OCT. (a) OCT mosaic image obtained by stitching 49 images. (b) Amplitude of the interferometric signal as a function of the optical path difference for blue square in (a). From these curve, the axial focus position and the axial resolution is measured. (c,d) 2D map of the axial focus shift and the axial resolution respectively. Scale bar, 500 μm.

found that this shift is induced by a slight tilt of the silicon mirror in the reference arm and not by the remote scanning system itself. Even though it can be ultimately corrected, note that this value is less than 0.3% of the FOV.

Here, we have demonstrated that similar features are obtained for all the images taken at different locations of the FOV. Hence, the remote scanning unit does not alter the nominal optical performances of the microscope, indicating that high-resolution imaging of large specimens is within reach with our approach.

2.5. *Imaging large biological specimens*

In the perspective of using our new approach to image a large and challenging biological sample, we applied our technique to an engineered heterogenous cell assembly composed of an endothelial vesseloid (i.e. engineered blood vessel) [13] and of encapsulated spheroids of liver cells [4]. The overall construct could then be regarded as a prototypal liver tissue architecture, with thick and diffusive micro-tissues in regard with hollow cell tubes with a lumen that may be further used to conduct blood diffusing molecules and circulating cells. Here, one needs both to visualize how the different building blocks (vesseloid and spheroids) are arranged respectively, and to gain insight into the internal structure of each component.

For a single detection angle (a static unitary FOV) we distinguish only a fraction of the vesseloid without figuring out the global structure of the sample (Fig. 5(b)). A 2.2×2.2 mm^2 FOV is acquired by stitching 7×7 wide-field images for various angles of the scanning unit. Such an extended FOV yields a more comprehensive picture of the sample and we can check that the long vesseloid is surrounded by packs of spheroids (Fig. 5(a)). After determining this overall arrangement of the tissue building blocks, we see that not all the regions are equally interesting. To gain efficiency, we decided to focus on the more relevant and optically challenging regions of interest and perform detailed investigation with the FF-OCT mode. This mode is complementary

Biomedical Optics EXPRESS

to the wide field mode as it overcome the lack of optical sectioning required for volumetric imaging [14].

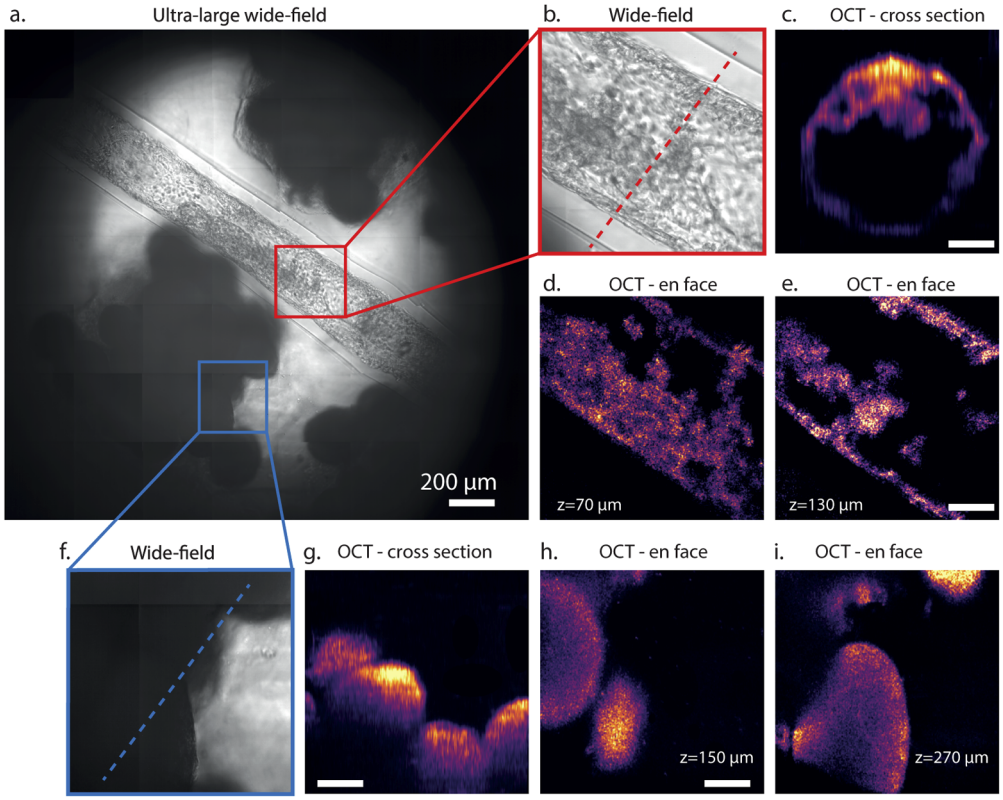

Fig. 5. Remote scanning applied to a large sample made of a vessel surrounded by spheroids.(a) Ultra-large FOV in wide-field microscopy obtained by stitching 7×7 images. (b) Single wide-field image corresponding to the red square in (a). Cellular information is clearly visible on the vesseloid. (c) Cross section image obtained with full-field OCT. It corresponds to the red dotted line in (b). (d,e) En face OCT image of the vessel obtained at depth z=70 and z=130 μm respectively. (f) Wide-field image corresponding to the blue square in (a). (g) Cross section image corresponding to the blue dotted line in (g). (h,i) En face OCT images of the same area at depth z=150 and 270 μm respectively. Scale bar, 100 μm.

Here, we focused on a vessel section and an ensemble of packed spheroids (respectively red and blue square on Fig. 5(a)). A z-stack is acquired with a 5 μm step on each of these areas. These two volumes are obtained without moving the sample, by just adjusting the scanning unit for setting the lateral location and the reference mirror for setting the depth. On the first region, en face OCT images taken at 70 and 130 μm display different tube widths and inhomogeneous thicknesses (see Fig. 5(d,e)). This complexity is also visible on the cross section image (Fig. 5(c)). We recognize the characteristic tubular shape of the vessel and thicker structures on the top part. That are the reminiscent shadows of supernumerary cells, that would be washed out upon perfusion. The strengths of FF-OCT are even more striking when imaging the stacks of multicellular spheroids. Indeed, while a contrasted image of a single spheroid is difficult to obtain by wide-field microscopy due to the highly scattering and absorbing properties of the spheroid, the loss of information becomes critical when spheroids are densely packed (Fig. 5(f)). From en face OCT images taken at 150 and 270 μm (see Fig. 5(h,i)) we see that several spheroids are

Biomedical Optics EXPRESS

indeed packed in the dark area of the wide-field image. These spheroids are of different sizes and located at different depths. A cross section image corresponding to the blue dotted line in Fig. 5(f) validates this observation (see Fig. 5(g)). We clearly see the volumetric arrangement of the capsules over 300 μm axially. Notably, even capsules on top of each other can be imaged.

3. Discussion

The remote scanning unit we added on our apparatus provides a large increase of the lateral FOV obtained with both the wide-field and the FF-OCT mode. Compared to conventional sample scanning, our method has the advantage of keeping the sample static but has also some limitations. Firstly, while sample scanning can potentially achieve an infinite FOV, our approach is limited to the area detected by the objective. Secondly, optical performances such as light collection and spatial resolution are degraded on the sides of the mosaic image. This effect is not observed in sample scanning as the area detected by the camera is always centered on the optical axis of the MO. Finally, this increase in information requires to make concession in terms of temporal resolution. There is a linear relationship between the number of frames, or acquisition duration, and the amount of data. Actually, the same trade-off occurs when the sample is moved directly using a motorized stage. Yet, in our approach we move the complexity from the sample plane to the detection unit of the microscope. Given the magnification of the current system, similar stroke is required for sample scanning or angular scanning (see Appendix D). In other words, if the same actuator is used in both cases, our approach will present similar performances than physically moving the sample stage. However, angular scanning implies to displace only a mirror mount which is much lighter compared to a bulky sample stage. For this reason, angular scanning is intrinsically much faster than mechanical scanning. For instance, it takes approximately 1 minute to acquire the ultra-large FOV in the wide-field mode in the current configuration. By replacing the motorized mounts by galvanometric mirrors, this acquisition time can be reduced at least by one order of magnitude.

As our approach aims to acquire sequentially the total amount of spatial information transmitted by the MO, one could argue that a more straightforward solution would be to increase the number of pixels of the camera. This is valid up to a certain point. Cameras with higher number of pixels exist but there are usually expensive and even the best ones cannot match the SBP of the most effective MO. Indeed, not all the MO transmits the same amount of information. This quantity depends on the field number (FN), the magnification (Mag) and the NA of a MO as follows [15]:

$$SBP = 4 \times \frac{\left(\frac{FN}{Mag}\right)^2}{\left(\frac{\lambda}{2NA}\right)^2} \tag{1}$$

Using this equation, the SBP for several MO is estimated for λ=650 nm and given in the Table 1. From this table, we first see that low magnification MO usually provides a higher SBP than high magnification ones. For instance, using a 4X and 0.2 NA can lead to SBP larger than 45 Mpixels, while a conventional 60X with NA=0.85 has only 5 Mpixels. In the latter case, the benefits of our approach would be very limited as the SBP roughly match the number of pixels of a conventional camera. On the contrary, no current camera can match the SBP of objectives recently developed for multi-photon and light sheet microscopy which offer an excellent light collection and spatial resolution with a moderate magnification [16]. In the case of the Nikon N16XLWD-PF, the collection of approximately 100 frames using the remote scanning principle would provide a 2 mm FOV with a 400 nm resolution.

From this table, the second thing we can learn is that the SBP of our microscope is still lower than the theoretical SBP of the MO. Indeed, we acquired only 75 % of the 21 Mpixels. This number is mostly limited by a small amount of clipping in both the illumination and the detection of our system (see Appendix D). In addition, field number of optical elements are indications

Biomedical Optics EXPRESS

Table 1. Spatial bandwidth product for various microscope objectives used in wide-field microscopy and FF-OCT.

Microscope objective	NA	SBP (Megapixels)
Thorlabs TL4X-SAP X4	0.2	45
Olympus UMPLFLN 10X	0.3	21
Olympus UMPLFLN 20X	0.5	15
Olympus UMPLFLN 40X	0.8	9
Nikon CFI Super FLuor X60	0.85	5
Nikon N16XLWD-PF 16X	0.8	97
Olympus XLUMPLFLN X20	1	46
Olympus XLPlan N 25X	1.05	22

given by the manufacturers and we do not know in which extent theoretical performances can be obtained.

An other strategy to increase the amount of information collected by a microscope is to use an array of cameras, as proposed in a recent work [17]. While there is no trade-off between temporal resolution and information with this approach, its complexity and its cost can be an obstacle to its dissemination. An elegant alternative consists in the acquisition of low magnification images obtained for various illumination angles. High resolution images over the entire FOV are then obtained thanks to a stitching operation in the Fourier space [18,19]. However, this technique called ptychography is mostly used in the transmission mode, and thus non-compatible with thick biological tissues. In addition to its simplicity, our approach offers flexibility as we can tune the number of acquired frames depending on the MO we use and match in each case its SBP. In the case of a non-continuous specimen, there is also the possibility to scan only few regions of interest. This would be similar to a wide-field version of random access scanning microscopy [20].

Finally, as we were interested in imaging specimens sensitive to motion and large 3D scattering structures without any label we limited this work on extending the FOV only in the case of wide-field microscopy and FF-OCT. Yet, our approach is not limited to these two imaging techniques and the remote scanning approach can be applied to all camera based or wide-field microscopic techniques. In particular, we believe our approach is of interest for differential interferometric contrast microscopy [21] and wide-field fluorescence microscopy [22]. In the latter case, this feature could be of interest to capture neuron activity on large parts of the mouse cortex.

4. Conclusion

In this work, we have combined a remote scanning mechanism with a FF-OCT system to perform volumetric imaging over large scales without moving the sample in any dimension. More precisely, the remote scanning mechanism allows to largely increase the lateral FOV of the microscope without sacrificing the lateral resolution. By collecting frames for various positions of the scanning unit, we imaged a FOV up to 2.2×2.2 mm^2 with a 1.1 μm resolution. We demonstrated the benefits of our approach on both wide-field microscopy and FF-OCT. Our method is particularly valuable when imaging specimens that are fragile or sensitive to motion.

Appendix A : Acquisition of the electromagnetic field

In full-field optical coherence tomography, it is necessary to measure the field from intensity only measurements. In this work, we adopted a triangular 5 phases stepping approach for the

Biomedical Optics EXPRESS

interferometric measurement. It consists in modulating the mirror position in triangles with a frequency equals to the tenth of the camera frequency [23,24]. From a cycle, we extract two measurements of the complex field, one for the ascending part of the cycle and one for the descending part. From 5 intensity images, the amplitude and the phase can be calculated as follows :

$$A = \sqrt{4(I_2 - I_4)^2 + (I_1 - 2I_3 - I_5)^2} \tag{2}$$

and

$$\phi = -\text{atan}\left(\frac{2(I_2 - I_4)}{I_1 - 2I_3 - I_5}\right). \tag{3}$$

Appendix B : Sample preparation

The super-assembly of Vesseloids and spheroids was obtained by positioning both tissue blocks within a hydrogel mold (2% agarose) casted so that a groove receive the Vesseloid and that deep wells can fit a superposition of up to 3 spheroids on top of each other. The spheroids and the Vesseloids were obtained with the Cellular Capsule Technology, used to produce either spherical hollow alginate capsules [4] or meter-long tubular capsules [13]. In the present study, the cells grown in the spherical capsules were the hepatocarcinoma cell line HuH6. Both spheroids and Vesseloids were fixed overnight in 4% PFA before being positioned in the agarose mold to prevent tissue degradation.

Appendix C : Image processing

To stitch the different images into the ultra-large FOV, we calibrated the 2D motorized motor using the USAF resolution target. Once the relationship between tilt-angle in the Fourier space and pixel shift in the image plane is known, a simple Matlab script was used to perform this operation. Visualizations were performed using Fiji [25].

Appendix D : Performances of the apparatus

Quality of the image depending on the position in the field of view

Here, we want to check if the remote scanning affects the transverse resolution and light collection depending on the location inside the microscope FOV.

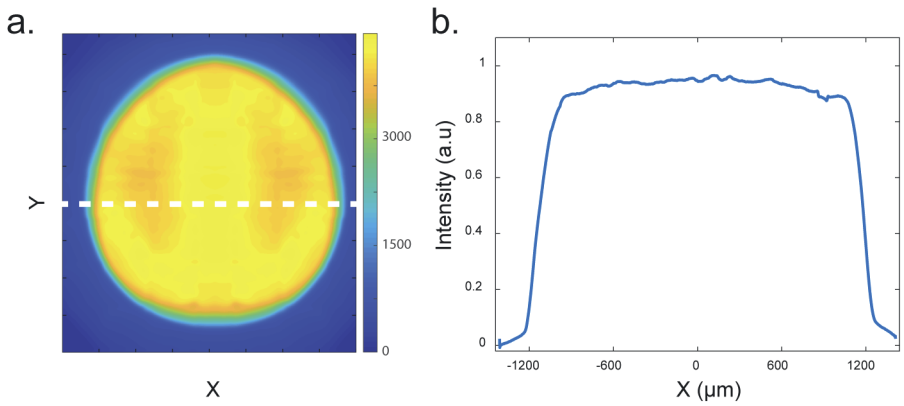

Fig. 6. (a) 2D map of the collection efficiency of the system measured with a mirror as a sample. (b) Plot profile of the collection efficiency corresponding to the white dashed line in (a).

Biomedical Optics EXPRESS

To first estimate the light collection efficiency, we acquire a mosaic image with a mirror as a sample. As seen on Fig. 6, the light collection is constant over roughly 2.2 mm and then falls off quickly.

Then, in order to estimate the spatial resolution of our system, we imaged 1 μm beads dispersed in an agarose gel and mounted on a glass slide. As seen on Fig. 7, there is no notable degradation of the transverse resolution inside the area where the light collection is constant. For distances larger than 1.1 mm from the center of the FOV, aberrations start to degrade the resolution and the system is not diffraction-limited anymore.

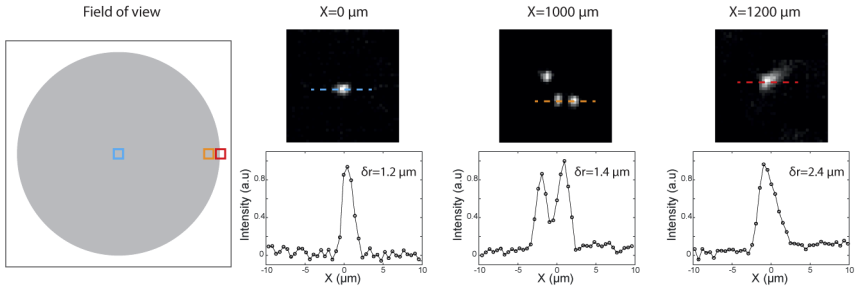

Fig. 7. Spatial resolution of the system depending on the location inside the microscope FOV. Measurements were performed using 1 μm latex beads dispersed in agarose.

Reproducibility of the scanning mechanism

Given the magnification of the system in its current configuration, similar stroke is required for sample scanning or angular scanning. Indeed, in the Fourier plane of the MO, the angle θ_{FOV} coming from a point at a position ΔX_{F0V} from the center of the FOV is given by

$$\tan(\theta_{FOV}) = \frac{\Delta X_{F0V}}{f} \tag{4}$$

with f the focal length of the MO. To compensate from this angle and image this object at the center of the camera, a tilt θ_m of the mirror has to be applied:

$$\tan(\theta_m) = \frac{\tan(\theta_{FOV})}{2} = \frac{X_m}{L} \tag{5}$$

with X_m the displacement produced by the actuator on the mirror mount and L the length of the mount. By using the small angles approximation, we obtain the following relationship between the displacement in the focal plane and the one that should be applied on the mirror mount:

$$X_m = \Delta X_{FOV} \times \frac{L}{2f} \tag{6}$$

In our case, f = 18 mm and L = 44 mm, so $X_m \sim \Delta X_{FOV}$. This means that if we use the same actuator in both cases, our system will present similar performances than physically moving the sample stage. However, angular scanning only requires to displace a mirror mount which is much lighter compared to a bulky sample stage. In theory, our approach allows to use relatively cost-effective actuators.

In practice, the actuators we used cost around 600 euros each (Z812B, Thorlabs). We tested the reproducibility of our apparatus by moving actuators in both direction by 1 mm back and forth. After each round trip, an image was captured and compared to the initial one by using a subpixel image registration algorithm [26]. As seen on Fig. 8, the error is significantly below 1 pixel which is a satisfying performance.

Biomedical Optics EXPRESS

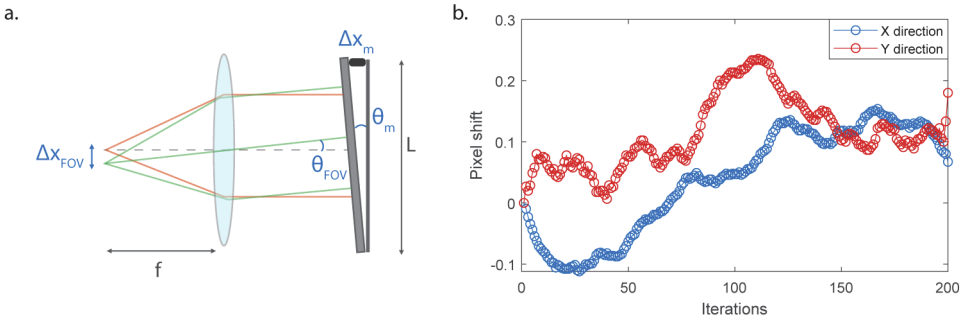

Fig. 8. (a) Sketch of the microscope objective and the scanning mirror and the corresponding angles and distances. (b) Reproducibility of the angular scanning method for both directions.

Funding

Agence Nationale de la Recherche (ANR- 7-CE30-0007-03, ANR-17- CE18-0026-02, ANR-17-CE13-0012-01); Ligue Contre le Cancer; Canceropole GSO.

Acknowledgements

The authors thank M. Caumont and A. Mombereau for spheroids production, N. Courtois-Allain and F. Saltel for providing us the HUH6 cell line and Pierre Bon for fruitful discussions and critical reading.

Disclosures

The authors declare no conflicts of interest.

References

1. A. W. Lohmann, R. G. Dorsch, D. Mendlovic, Z. Zalevsky, and C. Ferreira, "Space-bandwidth product of optical signals and systems," J. Opt. Soc. Am. A **13**(3), 470–473 (1996).
2. W. Lukosz, "Optical systems with resolving powers exceeding the classical limit," J. Opt. Soc. Am. **56**(11), 1463–1471 (1966).
3. G. McConnell, "Video-rate gigapixel imaging of the brain," Nat. Photonics **13**(11), 732–734 (2019).
4. K. Alessandri, B. R. Sarangi, V. V. Gurchenkov, B. Sinha, T. R. Kießling, L. Fetler, F. Rico, S. Scheuring, C. Lamaze, A. Simon, S. Geraldo, D. Vignjević, H. Doméjan, L. Rolland, L. Funfak, J. Bibette, N. Bremond, and P. Nassoy, "Cellular capsules as a tool for multicellular spheroid production and for investigating the mechanics of tumor progression in vitro," Proc. Natl. Acad. Sci. **110**(37), 14843–14848 (2013).
5. K. Alessandri, M. Feyeux, B. Gurchenkov, C. Delgado, A. Trushko, K.-H. Krause, D. Vignjević, P. Nassoy, and A. Roux, "A 3d printed microfluidic device for production of functionalized hydrogel microcapsules for culture and differentiation of human neuronal stem cells (HNSC)," Lab Chip **16**(9), 1593–1604 (2016).
6. P. Van Liedekerke, J. Neitsch, T. Johann, K. Alessandri, P. Nassoy, and D. Drasdo, "Quantitative agent-based modeling reveals mechanical stress response of growing tumor spheroids is predictable over various growth conditions and cell lines," PLoS Comput. Biol. **15**(3), e1006273 (2019).
7. B. Potsaid, Y. Bellouard, and J. T. Wen, "Scanning optical mosaic scope for micro-manipulation," in *Int. Workshop on Micro-Factories (IWMF02)*, (Citeseer, 2002), pp. 85–88.
8. B. Potsaid, Y. Bellouard, and J. T. Wen, "Adaptive scanning optical microscope (asom): a multidisciplinary optical microscope design for large field of view and high resolution imaging," Opt. Express **13**(17), 6504–6518 (2005).
9. E. Beaurepaire, A. C. Boccara, M. Lebec, L. Blanchot, and H. Saint-Jalmes, "Full-field optical coherence microscopy," Opt. Lett. **23**(4), 244–246 (1998).
10. A. Dubois, L. Vabre, A.-C. Boccara, and E. Beaurepaire, "High-resolution full-field optical coherence tomography with a linnik microscope," Appl. Opt. **41**(4), 805–812 (2002).
11. E. J. Botcherby, R. Juskaitis, M. J. Booth, and T. Wilson, "Aberration-free optical refocusing in high numerical aperture microscopy," Opt. Lett. **32**(14), 2007 (2007).
12. J. Scholler, K. Groux, O. Goureau, J.-A. Sahel, M. Fink, S. Reichman, C. Boccara, and K. Grieve, "Dynamic full-field optical coherence tomography: 3d live-imaging of retinal organoids," *arXiv preprint arXiv:1912.04052* (2019).

Biomedical Optics EXPRESS

13. L. Andrique, G. Recher, K. Alessandri, N. Pujol, M. Feyeux, P. Bon, L. Cognet, P. Nassoy, and A. Bikfalvi, "A model of guided cell self-organization for rapid and spontaneous formation of functional vessels," Sci. Adv. **5**(6), eaau6562 (2019).
14. A. Badon, A. C. Boccara, G. Lerosey, M. Fink, and A. Aubry, "Multiple scattering limit in optical microscopy," Opt. Express **25**(23), 28914–28934 (2017).
15. J. R. Bumstead, J. J. Park, I. A. Rosen, A. W. Kraft, P. W. Wright, M. D. Reisman, D. C. Côté, and J. P. Culver, "Designing a large field-of-view two-photon microscope using optical invariant analysis," Neurophotonics **5**(2), 025001 (2018).
16. A. Singh, J. D. McMullen, E. A. Doris, and W. R. Zipfel, "Comparison of objective lenses for multiphoton microscopy in turbid samples," Biomed. Opt. Express **6**(8), 3113–3127 (2015).
17. J. Fan, J. Suo, J. Wu, H. Xie, Y. Shen, F. Chen, G. Wang, L. Cao, G. Jin, Q. He, T. Li, G. Luan, L. Kong, Z. Zheng, and Q. Dai, "Video-rate imaging of biological dynamics at centimetre scale and micrometre resolution," Nat. Photonics **13**(11), 809–816 (2019).
18. L. Tian, Z. Liu, L.-H. Yeh, M. Chen, J. Zhong, and L. Waller, "Computational illumination for high-speed in vitro fourier ptychographic microscopy," Optica **2**(10), 904–911 (2015).
19. G. Zheng, R. Horstmeyer, and C. Yang, "Wide-field, high-resolution fourier ptychographic microscopy," Nat. Photonics **7**(9), 739–745 (2013).
20. R. Salome, Y. Kremer, S. Dieudonne, J.-F. Léger, O. Krichevsky, C. Wyart, D. Chatenay, and L. Bourdieu, "Ultrafast random-access scanning in two-photon microscopy using acousto-optic deflectors," J. Neurosci. Methods **154**(1-2), 161–174 (2006).
21. N. T. Shaked, Z. Zalevsky, and L. L. Satterwhite, *Biomedical Optical Phase Microscopy and Nanoscopy* (Academic Press, 2012).
22. A. I. Mohammed, H. J. Gritton, H.-a. Tseng, M. E. Bucklin, Z. Yao, and X. Han, "An integrative approach for analyzing hundreds of neurons in task performing mice using wide-field calcium imaging," Sci. Rep. **6**(1), 20986 (2016).
23. A. Federici, H. S. G. da Costa, J. Ogien, A. K. Ellerbee, and A. Dubois, "Wide-field, full-field optical coherence microscopy for high-axial-resolution phase and amplitude imaging," Appl. Opt. **54**(27), 8212–8220 (2015).
24. O. Thouvenin, "Optical 3d imaging of subcellular dynamics in biological cultures and tissues: applications to ophthalmology and neuroscience," Ph.D. thesis, Université Sorbonne Paris Cité (2017).
25. J. Schindelin, I. Arganda-Carreras, E. Frise, V. Kaynig, M. Longair, T. Pietzsch, S. Preibisch, C. Rueden, S. Saalfeld, B. Schmid, J.-Y. Tinevez, D. J. White, V. Hartenstein, K. Eliceiri, P. Tomancak, and A. Cardona, "Fiji: an open-source platform for biological-image analysis," Nat. Methods **9**(7), 676–682 (2012).
26. M. Guizar-Sicairos, S. T. Thurman, and J. R. Fienup, "Efficient subpixel image registration algorithms," Opt. Lett. **33**(2), 156–158 (2008).